Geology, Geophysics & Environment 2026, vol. 52 (1): 69–85

Integration of MASW and ERT methods for site characterisation: A case study from Czernichów (Southern Poland)

Kamil Cichostępski[1], Grzegorz Bania[2], Aleksandra Borecka[3]

[1] *AGH University of Krakow, Faculty of Geology, Geophysics and Environmental Protection, Krakow, Poland, e-mail: kcichy@agh.edu.pl (corresponding author), ORCID ID: 0000-0001-7982-4763*
[2] *AGH University of Krakow, Faculty of Geology, Geophysics and Environmental Protection, Krakow, Poland, ORCID ID: 0000-0002-9661-8184*
[3] *AGH University of Krakow, Faculty of Geology, Geophysics and Environmental Protection, Krakow, Poland, ORCID ID: 0000-0001-8735-4992*

Received: 13 January 2026; accepted: 26 March 2026; first published online: 28 April 2026

Abstract: The paper presents an integrated use of multichannel analysis of surface waves (MASW) and electrical resistivity tomography (ERT) to characterise the physical properties of near-surface materials, identify subsurface structures, and estimate the depth to bedrock in a planned construction area near Czernichów, close to Krakow (southern Poland). The study shows that integrating MASW and ERT provides a cost-effective and complementary approach to subsurface characterisation, delivering more reliable and less ambiguous interpretations than when the methods are applied independently, thereby reducing the need for expensive and invasive in situ geotechnical investigations. Particular emphasis is also placed on the methodological aspects of both methods. The study site is located on an alluvial plain composed of alluvial soils, sands, sand–gravel mixtures, and silty clays overlying limestone bedrock. Geophysical data were collected along five profiles. The resulting shear wave velocity models and the inverse model resistivity sections show good agreement with borehole data. The study area is characterised by a wide range of physical parameters derived from both methods. The MASW survey enabled recognition of the subsurface down to the bedrock, revealing four seismic layers differing in S-wave velocity. Nevertheless, the MASW inversion did not provide reliable estimates of the limestone S-wave velocity, although it successfully delineated its depth and morphology. The ERT survey identified three geoelectrical layers and proved to be more effective in resolving shallow geological structure, particularly in identifying the boundaries between alluvial soils and sand–gravel mixtures, whereas the depth and morphology of the limestone bedrock were constrained primarily by MASW.

Keywords: near-surface geophysics, multichannel analysis of surface waves, electrical resistivity tomography, integrated interpretation, site characterisation

INTRODUCTION

A key factor in designing building foundations is gaining a thorough understanding of the subsurface geology and the mechanical characteristics of the ground (Clayton et al. 1995). Understanding the geotechnical characteristics of subsurface materials, such as soil strength, is essential. Several methods can be applied to evaluate subsurface conditions. In most cases, research is conducted

using invasive geotechnical methods that measure the resistance of the soil to penetration, such as the standard penetration test (SPT) or cone penetration test (CPT, CPTu). Nevertheless, the key disadvantage of intrusive approaches is that they supply data solely from sampling locations. Covering a large area, especially in regions with suspected lateral facies variations or complex geological structures, requires numerous investigations. This limitation can be addressed by implementing complementary geophysical surveys. Incorporating geophysical measurements into geotechnical investigations helps to reduce the number of mechanical tests needed, thereby lowering project costs.

Geophysical methods are non-invasive and make it possible to determine quasi-continuous variations in soil properties. They are faster and more cost-effective than conventional geotechnical methods and enable the detection of subsurface anomalies that may not be identified through point measurements (Cosenza et al. 2006, Hubbard 2009). Geophysical techniques that can assist in characterising the near-surface zone include, for example, seismic refraction tomography (Golonka et al. 2022, Cichostępski et al. 2024), multichannel analysis of surface waves (Park 2013), high-resolution reflection profiling (Cichostępski et al. 2019a, 2019b, Cichostępski & Dec 2021), electrical resistivity tomography (Bania & Woźniak 2022), ground-penetrating radar (Akinsunmade et al. 2020), and microgravimetry (Gołębiowski et al. 2018). Such geophysical techniques are very efficient at identifying underground structural irregularities that may threaten the stability and safety of foundation design. Selecting a method depends on the survey objectives, the geological conditions of the site, and the required solution. Although geophysical methods have limitations, such as restricted penetration depth, a decrease in detail with increasing depth, and dependence on particular physical characteristics of the underground materials, their advantages largely compensate for the limitations of conventional geotechnical methods. To reduce the limitations and ambiguity associated with relying on a single geophysical technique, it is strongly recommended to combine multiple methods. In recent years, multichannel analysis of surface waves (MASW) and electrical resistivity tomography (ERT) have gained routine application in geotechnical studies, enabling the mapping of 2D subsurface structures throughout the surveyed area (Adenuga & Popoola 2020, Zhao et al. 2020). Combining the MASW and ERT methods can address challenges commonly faced in near-surface geophysical investigations.

MASW is a non-invasive seismic technique that analyses surface waves to estimate shear-wave velocities, usually within the upper several tens of metres of the subsurface. It was introduced in 1999 by scientists at the University of Kansas (Park et al. 1999, Xia et al. 1999). MASW measurements employ seismic waves generated by a hammer or weight drop that propagate through the subsurface. The velocity of propagation varies depending on the properties of the medium, such as the lithology and its textural and structural characteristics. Generally, the denser and more consolidated the material, the faster the seismic waves travel (Olona et al. 2010). Over the last two decades, the use of MASW has increased, as S-wave velocity is one of the most important geotechnical parameters in civil engineering (Park 2013). Furthermore, the S-wave velocity correlates well with the blow counts parameter obtained from a in situ standard penetration test (Mayne & Rix 1993, Samui & Sitharam 2010). Compared to the S-wave refraction tomography method, which also provides S-wave velocities, MASW is much easier to perform and provides reliable and accurate results. S-wave refraction is often limited by a low signal-to-noise ratio, whereas MASW can easily achieve high signal quality. Moreover, MASW can be applied at sites where a shallow groundwater level is expected, as this method is not sensitive to the presence of water and can effectively resolve subsurface geological structure beneath it, especially when loose sediments are present. Under such conditions, the commonly used seismic P-wave refraction tomography method may prove ineffective, thereby limiting its applicability for site characterisation. This is why the MASW method is widely applied in various geotechnical, environmental and engineering studies such as soil characterisation (Foti et al. 2011), bedrock mapping (Miller et al. 1999), seismic site characterisation (Craig & Hayashi 2016), levee and dam assessment (Craig et al. 2021), fault zone mapping

(Ivanov et al. 2006), sinkhole detection (Park & Taylor 2010), landslides (Harba et al. 2019) and landfill characterisation (Naveen et al. 2021).

The ERT technique works by applying an electric current into the subsurface via electrodes and recording the resulting potential difference, which can be used to calculate the resistance and, consequently, resistivity. This method underwent significant development in the 1990s, driven by advances in the automation and computerisation of electrical resistivity measurements. During this period, the possibility of computer interpretation of this type of research data also appeared (Dahlin 1996). The ERT method provides the apparent resistivity distribution of the subsurface. This parameter characterises a heterogeneous geological medium and varies considerably, ranging from approximately 1 $\Omega \cdot m$ in saline and silty formations to several thousand ohm-metres in sediments such as dry sands or volcanic rocks (Loke 2018). Apparent resistivity is a complex parameter that depends on many factors, such as fluid content, water mineralisation, porosity, lithology, mineral composition, and pore filling. With knowledge of the media's resistivity ranges and borehole data from the area, the results can be interpreted as the lithology of the geological formations. Nowadays, the ERT technique is well established as the most popular and effective non-invasive method of electrical resistivity research techniques, allowing for the 2D/3D recognition of the geoelectrical structure of the near-surface zone and its monitoring in time (4D). ERT is widely applied in the general recognition of geological structure (see, e.g., Smith & Sjogren 2006, Ikhane et al. 2012, Woźniak et al. 2018, Woźniak & Bania 2019a, 2019b, Bania et al. 2024, Łój et al. 2025). Moreover, it is particularly suitable for characterising unconsolidated deposits of fluvial origin (see e.g., Matys Grygar et al. 2016, Akinbiyi et al. 2019), which exhibit high resistivity variability depending on the porosity, type of pore-filling medium (air/water), proportion of clay/sand material, and groundwater mineralisation (Telford et al. 1990).

The aim of this article is to present the effectiveness of integrated geophysical methods in the characterisation of subsurface media, and it focuses on the methodological aspects of both methods. The geophysical data used in this study were measured during surveys carried out prior to the geotechnical investigations for the planned construction in the vicinity of the village of Czernichów, near Krakow, southern Poland. The survey was designed as an initial stage of site characterisation, preceding geotechnical drilling and in situ testing. Its dual objective was to identify zones of interest for further testing and to constrain key subsurface physical parameters. The investigation focused on determining the physical properties of near-surface materials, mapping subsurface structures, and estimating the depth to bedrock as well as its morphological variability. To achieve this, MASW and ERT were applied in a complementary manner: MASW was intended to constrain the depth and morphology of the bedrock, whereas ERT was used primarily for detailed characterisation of the shallow overburden. It should be noted that part of the ERT data has previously been presented by Mościcki et al. (2014), who showed inverse model resistivity cross-sections for three of the five ERT profiles, whereas the structural maps, including the interpreted tops of lithological layers, were based on all five profiles. In this study, these data are revisited and fully reprocessed, visualised, and interpreted using up-to-date software tools. The earlier processing (Mościcki et al. 2014) was based primarily on the default settings of the Res2Dinv software, except for the application of the robust inversion option, whereas the present reprocessing involved testing selected inversion options and applying a customised set of inversion parameters. The primary goal of this reanalysis was to compare the ERT results with previously unpublished MASW data as part of an integrated interpretation. This integrated approach enabled the development of a more reliable and less ambiguous model of the geological subsurface in the study area.

MATERIALS AND METHODS

Study area

The research site is situated in Czernichów village, close to the Vistula River in southern Poland, around 20 km southwest of Krakow (Fig. 1). The site is relatively flat and covered with grass. Local geology consists of soft alluvial Holocene sediments and clastic Miocene deposits overlying solid Upper Jurassic carbonate bedrock (Golonka 1981).

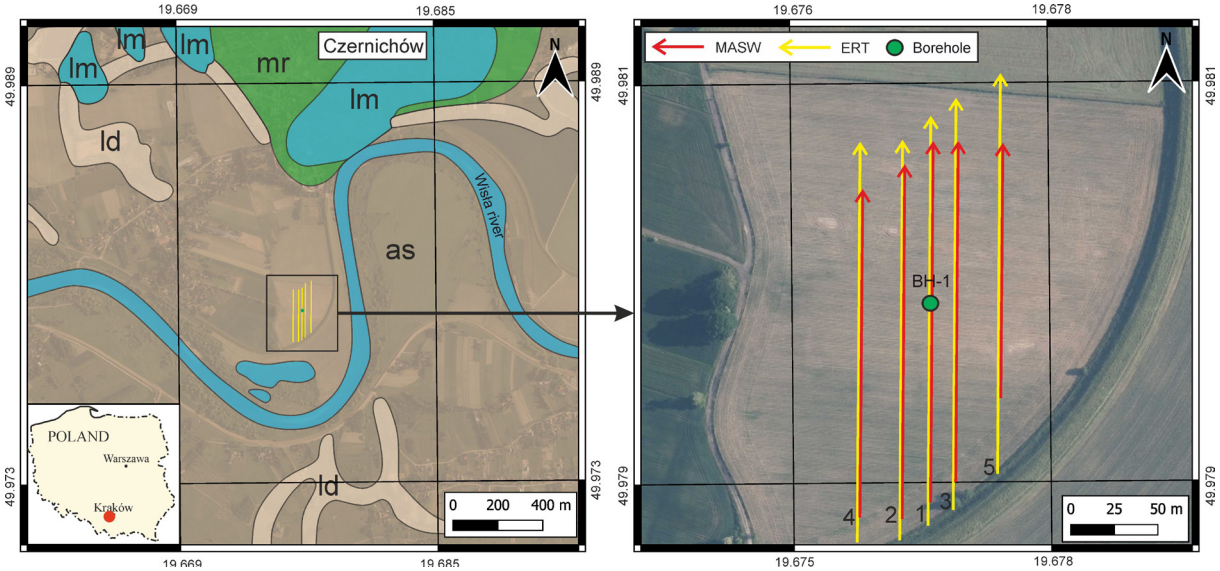

Fig. 1. *Lithological map of the study area (modified after Ryłko & Paul 2013) showing the locations of geophysical profiles along which MASW and ERT measurements were conducted. Explanations: 1–5 – geophysical profiles, lm – Jurassic limestones, mr – Cretaceous marls, as – alluvial soils, ld – lacustrine deposits*

The Upper Jurassic deposits consist of light-grey, massive siliceous limestones, with occasional occurrences of black flint. These formations are intersected by numerous faults, forming tectonic horsts and grabens of various sizes. Exposures of limestone can be observed in the northern part of the study area. Miocene sediments are mainly grey, silty clays with silt laminations, filling irregularities on the limestone surface and tectonic grabens. The investigation area is part of the Vistula River alluvial plain, composed of unconsolidated Holocene clastic sediments overlying the Miocene strata. The basal section of the Holocene profile is mainly composed of sandy gravels and gravels, grading upward into medium sands. The overlying sediments display alternating layers with varying grain sizes, such as silts, silty sands, medium sands, dusts, and sandy dusts (Golonka 1981, Borecka et al. 2014).

The groundwater table was encountered within Quaternary sandy-gravel deposits (Borecka et al. 2014). It forms a laterally continuous unconfined aquifer that is hydraulically connected to the nearby Vistula River. Owing to the close proximity of the river channel, groundwater level fluctuations are strongly correlated with variations in the river stage. During the acquisition campaign, groundwater was observed at a depth of approximately 6.1 m in borehole BH-1 (Fig. 2).

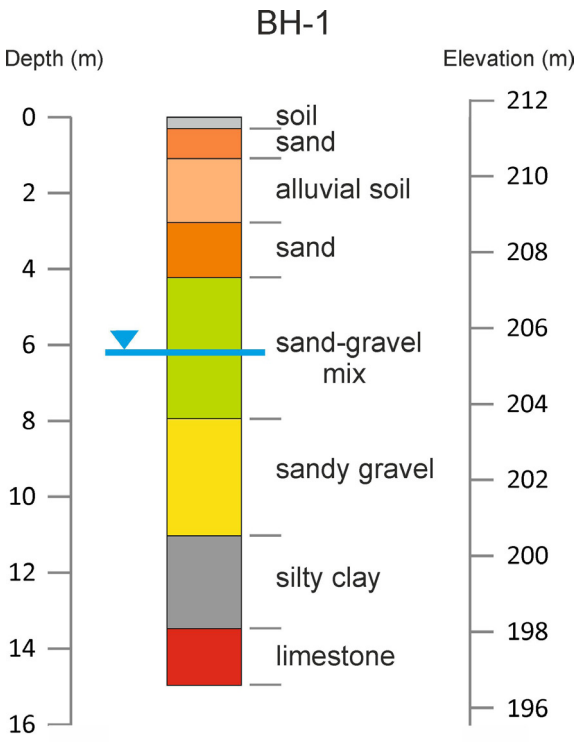

Fig. 2. *Lithology profile from BH-1. See Figure 1 for its location. The groundwater level was found at a depth of 6.1 m within a sand–gravel mix*

Methods

For the site characterisation in the study area, the multichannel analysis of surface waves (MASW) and electrical resistivity tomography (ERT) techniques were applied. Five parallel geophysical survey profiles were laid out across the planned foundation area (Fig. 1). MASW and ERT 2D measurements were acquired along these profiles. Borehole BH-1, located at the 130 m position along Profile 1, provided lithological information down to the bedrock (Fig. 2). The methodology of each geophysical method is presented in the following section.

Multichannel analysis of surface waves

Multichannel analysis of surface waves utilises the dispersive nature of surface waves (mainly the fundamental mode of Rayleigh waves), which exhibit the highest energy in seismic records. Dispersion refers to the phenomenon in which various frequencies propagate at different speeds (called phase velocities) in a heterogeneous medium (Park et al. 1999). This characteristic is thus utilised to derive a dispersion curve, representing the relationship between frequency and phase velocity. By applying an inversion process, these dispersion curves can be converted into a 1D shear-wave velocity profile with depth. Combining several 1D profiles then makes it possible to create a final pseudo-2D cross-section. (Xia et al. 2000).

Seismic data were collected along five profiles (Fig. 1) using a 24-channel Geometrics GEODE seismograph with 4.5 Hz vertical geophones spaced every 2 m. Only 19 geophones were available during the survey, which gives a total spread length of 38 m. Surface waves were generated using an 8 kg sledgehammer striking a polyethylene plate. A conventional *roll-along* acquisition technique was used, with the source placed 15 m ahead of the spread. After each shot, the spread was moved 10 m along the profile. The study area was characterised by low seismic noise. Nevertheless, up to five hammer strikes at each shot position were performed to enhance the signal-to-noise ratio. This allows the acquisition of high-quality data. The record length was 1 s, which was enough to record fully developed surface waves. The sampling interval was 1 ms. The lengths of the MASW-1, MASW-2 and MASW-3 profiles were 210 m, while the lengths of the MASW-4 and MASW-5 profiles were 140 m. The MASW data processing was carried out with the Geogiga Surface Plus software package (ver. 10.0, Geogiga Technology Corp.). The initial stage of data processing involved converting selected shot gathers from the time–distance (t–x) domain to the frequency–phase velocity (f–v) domain using the phase shift method (Park et al. 1999). For each record, the dispersion curve of the Rayleigh wave fundamental mode was interpreted and inverted individually to generate a 1D profile of V_S (S-wave velocity) variation with depth. The accurate interpretation of the dispersion curve is the most crucial part of this process. Proper interpretation requires dispersion curves to be smooth and continuous over the widest possible frequency range. The precision and clarity of the dispersion image are determined by the field data acquisition settings (Ivanov et al. 2008, Taipodia et al. 2018). The theoretical minimum wavelength and shallow depth resolution are influenced by the spacing between the geophones, while the maximum wavelength and depth of the investigation are determined by the geophones' natural frequency and the overall spread length. In general, however, the features of the dispersion image are strongly affected by local site conditions. For most of the acquired data, dispersion curves could be interpreted across a broad frequency range of 7–60 Hz. Below 7 Hz, the signal was blurred and unsuitable for interpretation. The initial models for inversion consisted of 9 layers. The thickness of each layer was determined using the formula:

$$H_{i+1} = H_i + 1.20 \quad (1)$$

where H_i is the thickness of the i^{th} layer. The thickness and depth penetration range was estimated based on the wavelength (velocity/frequency relationship) divided by 2 (Dal Moro 2014). The first layer thickness was assessed from the highest frequency of the dispersion picks, while the maximum depth was controlled by the lowest frequency picked on a given record.

The interpreted dispersion curves for all records were inverted using a genetic algorithm (GA). This technique is considered a global search

approach, capable of bypassing local minima that the conventional iterative non-linear least squares inversion may fall into. It is a reliable and robust method, which has been successfully used by numerous researchers for inverting dispersion curves (Yamanaka & Ishida 1996, Hayashi 2012). The genetic algorithm relies on three fundamental operations inspired by biological evolution: selection, crossover, and mutation (Boschetti et al. 1996). In this approach, geophysical properties like wave velocity, layer thickness, and density are considered as genes. Using a GA for the dispersion curve inversion requires minimal prior information and does not depend on the parameters needed for the forward modelling problem (Dal Moro et al. 2007). A notable drawback of the GA is its need for substantially more forward modelling than traditional methods.

The parameters used in the genetic inversion algorithm are listed below:

- iterations: 30;
- population: 128;
- crossover probability: 0.90;
- mutation probability: 0.020;
- seed: 80.

By inverting the interpreted dispersion curves, the S-wave velocity was estimated down to approximately 24 m. After inversion, the resulting 1D V_S model was positioned at the centre of the geophone spread. The root mean square error (RMSE) for all estimated V_S models was under 2.5%, indicating a high degree of reliability. The RMSE was calculated as the difference between the interpreted dispersion curve and the theoretical curve derived from the V_S model obtained through inversion (Xia et al. 1999).

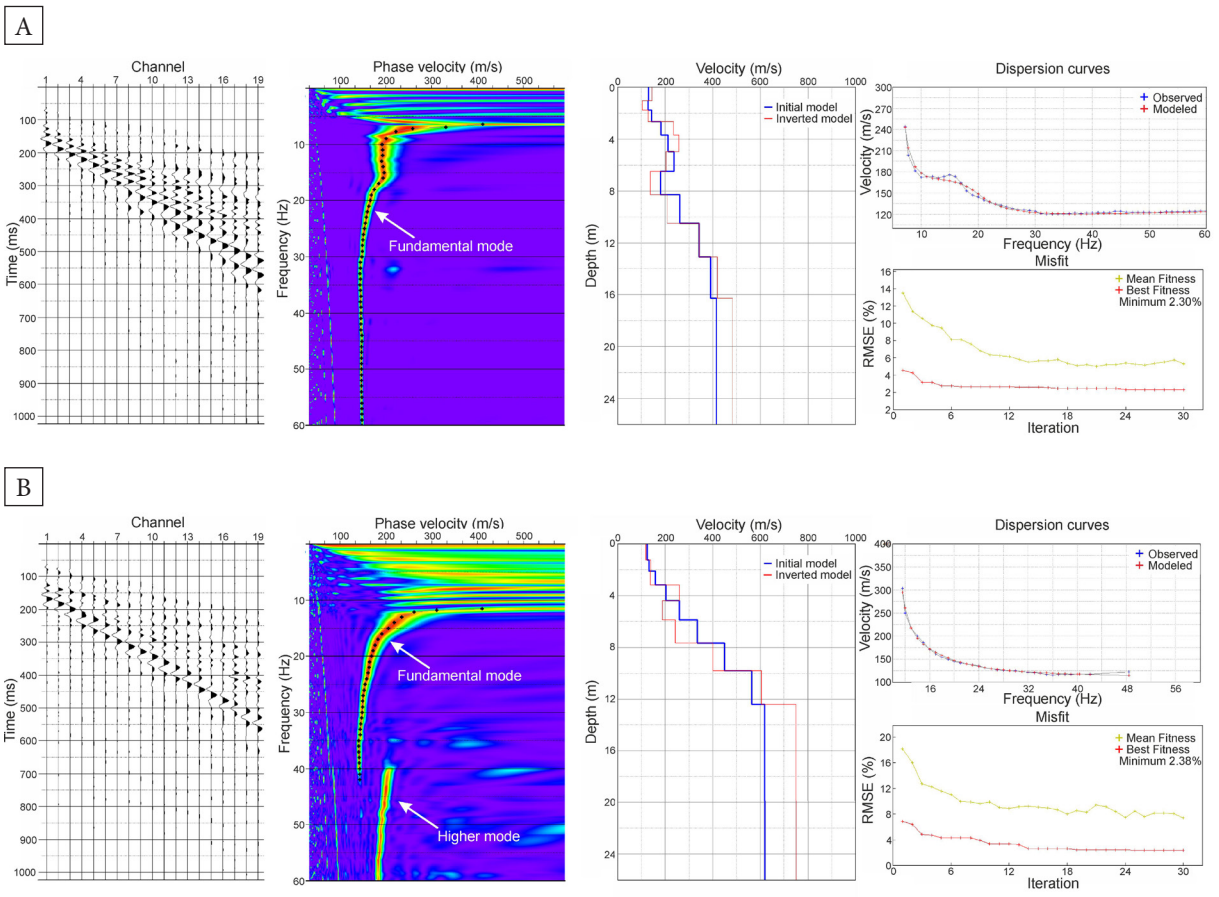

Fig. 3. *Representative shot gathers and their associated interpreted dispersion curves, together with the derived 1D S-wave velocity models through inversion: A) Shot #1 from the beginning of the MASW-1 profile; B) Shot #15 from the end of the MASW-3 profile. In panel A, the bedrock occurs at the greatest depth, while in panel B, it occurs at the shallowest depth within the study area*

Figure 3 presents two exemplary seismic records together with their spectral analyses and the resulting 1D shear-wave velocity models obtained through inversion. The final step involved interpolating 1D velocity models in sequential order along the given profiles to create a 2D S-wave cross-section. The resulting cross-sections were then smoothed using a mean filter with a horizontal window width of 5.

Electrical resistivity tomography

The ERT measurement technique usually involves placing several dozen electrodes at equal distances (Δx – spacing) and performing a series of electrical resistivity profiling in an automated manner (Burger et al. 2006) with selected measurement arrays. The result of ERT measurements is the so-called apparent resistivity pseudosection (ARP), where the vertical axis represents a parameter related to the measurement array size (half the spacing of the current electrodes, AB/2, or the so-called pseudo-depth), and the horizontal axis indicates the distance along the profile (Loke 2018). This pseudosection is subjected to quantitative analysis, i.e., geophysical interpretation (inversion).

Inversion involves choosing a discrete 2D resistivity model of the geological medium whose response to simulated measurements (theoretical ARP) closely matches the ARP recorded in field surveys. The accuracy of the inversion is assessed using the RMS error or the absolute error between the theoretical and field ARP (Loke 2018). By repeating this process many times (iterating), an inverse model resistivity section is obtained as a function of depth and distance on the profile. It is important to note that the resistivity distribution derived from the inversion does not necessarily represent the actual subsurface resistivity and should instead be considered as interpreted resistivity. This phenomenon arises due to the inherent non-uniqueness of the inversion process.

Electrical resistivity tomography was acquired along the same profiles as the MASW measurements (Fig. 1). In the measurements, the GDRM-VAR resistivity system with a set of 96 electrodes was employed. For all ERT profiles, a 1 m spacing (Δx) (distance between adjacent electrodes) was applied. This made it possible to construct a basic profile of 95 m in length (using the maximum number of electrodes) for all five survey lines. To achieve the desired length of the profiles, that is, 231 m, the *roll-along* technique was used. It involves successively moving the initial sections of cables with electrodes to the end of the current basic profile and then continuing the measurements (Dahlin 1996). This way, a profile of any length can theoretically be run. In this case, the overall single profile consisted of three basic sections (A, B, and C), with each subsequent section overlapping the previous one by approximately one-third of its length. The lengths of the individual sections, measured relative to the entire study profile, were as follows: A – 0–95 m, B – 64–159 m, and C – 136–231 m. This arrangement provided complete coverage of the apparent resistivity data both along the entire profile and across the desired depth range. The Wenner alpha array with parameters a = 1, 2, 3, 4, 5, 6, 8, 10, 13, and 16 Δx was applied. The Wenner array was selected due to its strong signal, low noise sensitivity, and highest vertical resolution, making it particularly effective for delineating layer boundaries in horizontally stratified geological settings. The chosen measurement sequence allowed for the acquisition of over 2,000 apparent resistivity values along each ERT survey line, providing dense spatial coverage and reliable data for subsequent inversion and interpretation. Additional information for all profiles is given in Table 1. The exact positions of the electrodes and the distance between them on the individual profiles were determined using geodetic measurements. Simultaneously, the elevation of each electrode along the ERT profiles was measured using geodetic levelling. The coordinates of characteristic points on individual survey lines were measured using a GNSS receiver.

Measurement data obtained during ERT surveys were inverted in the Res2Dinvx64 software (ver. 4.10.21, Aarhus Geosoftware). Numerous parameter configurations offered by the software were tested, and their own set was developed. Two basic inversion variants were analysed, i.e., *robust* (l_1-norm) and *smooth* (l_2-norm) (Loke et al. 2003). Finally, the *robust* inversion approach was selected, as the goal of the interpretation was to most accurately delineate the boundaries between

contrasting geoelectrical mediums on the obtained resistivity cross-sections (see, e.g. Elwaseif & Slater 2010, Bania & Woźniak 2022). The inversion mesh was created so that all model blocks were of equal width and there were two mesh nodes between adjacent electrodes. The *Use extended model* option, which is turned on by default, was also disabled, giving the inversion mesh a trapezoidal shape. Moreover, the influence of the model's boundary blocks on the inversion results was limited. It is important to note that this effect is fairly common, particularly when there are relatively large resistivity contrasts in the medium (above around 1:200). It appears as an artificial increase or decrease in the resistivity values of interpreted zones situated at the edges of the ERT sections (Loke 2018). This effect was mitigated by adjusting the default *Reduce effect of side blocks* setting to *Slight*, which also helped decrease the absolute error for the tested data. Other inversion options not mentioned in the paper were also tested.

After inversion, in the case of the ERT-3 survey line, additional filtering was applied using the *RMS error statistics* option (thanks to the excellent quality of the data, the remaining profiles did not require this step). A cutoff error of 20% was selected. This filtering enabled the removal of data points that showed relatively large discrepancies between the measured and calculated apparent resistivity values (Loke 2018). After filtration, the inversion of the ERT-3 dataset was performed once again. The high quality of the data and the filtering applied to the ERT-3 dataset granted the inverse model resistivity sections relatively small absolute error values (Table 1). With the applied methodology, the depth of investigation is approximately 10 m.

Table 1

Characteristics of field measurements and l_1-norm inversion results for the ERT method. For each profile, the effective number of electrodes (regarding roll-along overlaps) was 232, and the spacing was $\Delta x = 1$ m

ERT profile	Electrode no.	Data collected no.	Iterations no.	Absolute error [%]
ERT-1	96	2046	8	2.04
ERT-2		2048	8	1.89
ERT-3		2048	10	1.98
ERT-4		2048	9	2.62
ERT-5		2047	9	1.46

RESULTS AND DISCUSSION

MASW results

The MASW-1, MASW-2, MASW-3, MASW-4 and MASW-5 2D cross-sections along five geophysical profiles are presented in Figures 4A, 5A, 6A, 7A and 8A, respectively. The obtained S-wave velocities vary between 100 and 800 m/s, showing the variation in subsurface properties at the site designated for construction. The applied methodology makes it possible to recognise subsurface materials down to 24 m. All MASW 2D cross-sections show a similar image of the subsurface, where four distinct layers can be differentiated based on velocity contrasts (L1s – L4s seismic layers). The uppermost layer (L1s) indicates that the surface and near-surface materials possess very low S-wave velocities, around 120 m/s. This thin, continuous layer reaches up to 2 m in thickness. In the northern section of the study area, velocities within this layer drop to approximately 100 m/s. S-wave velocities in the second layer (L2s) are around 200 m/s. Across the study area, the layer's thickness decreases from approximately 12 m in the southern region to 3 m toward the north. Within this layer, a thin zone of relatively higher velocity (approx. 280 m/s) is embedded in lower-velocity sediments, although this sublayer is not visible in the westernmost profile (Fig. 7A). The third layer (L3s) shows S-wave velocities between 350 and 550 m/s, with the thickness reducing from 7 m in the south to 2 m in the northwest. The lowermost layer (L4s) has the highest S-wave velocities (exceeding 600 m/s), and its depth ranges from 22 m in the southern part of the area to 8 m in the north.

ERT results

The ERT-1, ERT-2, ERT-3, ERT-4 and ERT-5 2D cross-sections along five geophysical profiles are shown in Figures 4B, 5B, 6B, 7B and 8B, accordingly. The employed Wenner alpha array offers the highest signal-to-noise ratio and excellent vertical resolution. With an electrode spacing of 1 m, it enables precise imaging of the upper 10 m of the subsurface. The inverse model resistivity sections reveal that the resistivity values across the study area vary between 10 and 4,000 $\Omega \cdot$m, reflecting significant contrasts in subsurface conductivity.

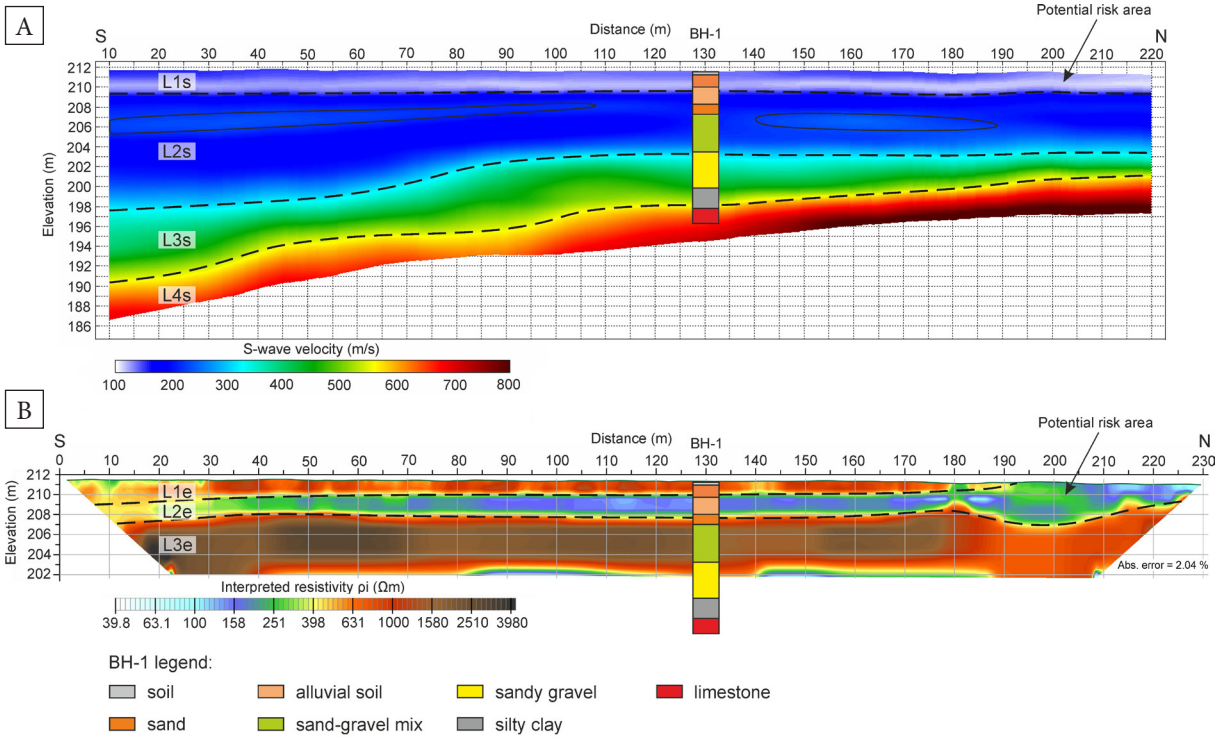

Fig. 4. *Results of the MASW-1 (A) and ERT-1 (B) geophysical measurements. Explanations: L1s – L4s – interpreted seismic layers, L1e – L3e – interpreted geoelectrical layers. The oval within L2s indicates a sublayer characterised by relatively higher S-wave velocities*

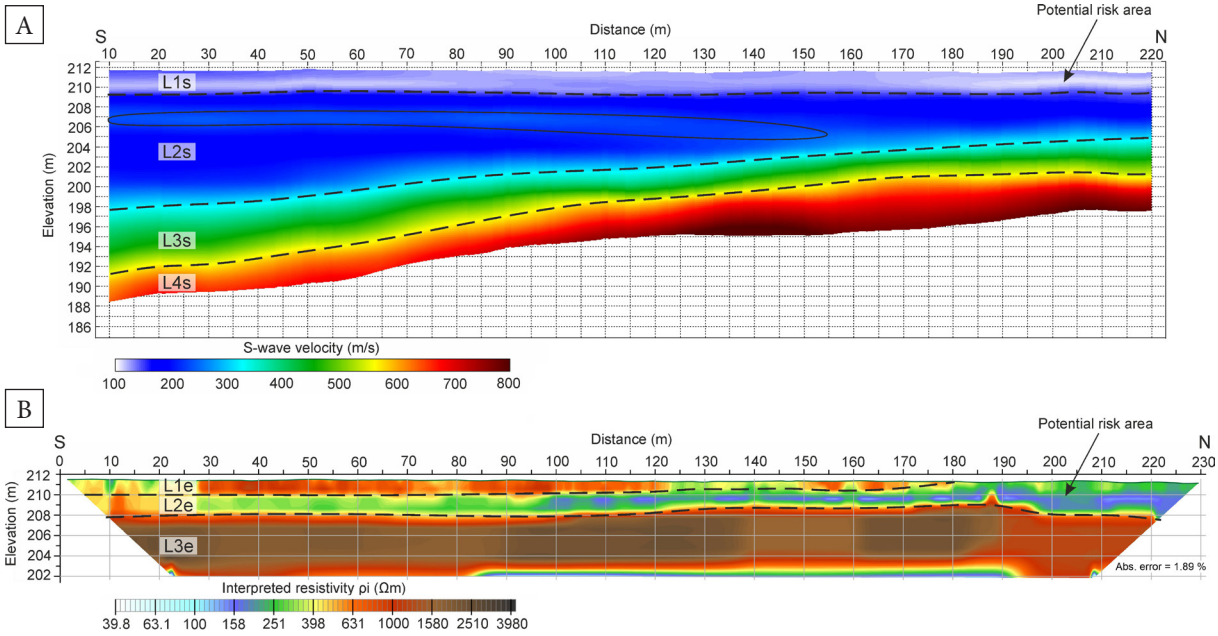

Fig. 5. *Results of the MASW-2 (A) and ERT-2 (B) geophysical measurements. Explanations: L1s – L4s – interpreted seismic layers, L1e – L3e – interpreted geoelectrical layers. The oval within L2s indicates a sublayer characterised by relatively higher S-wave velocities*

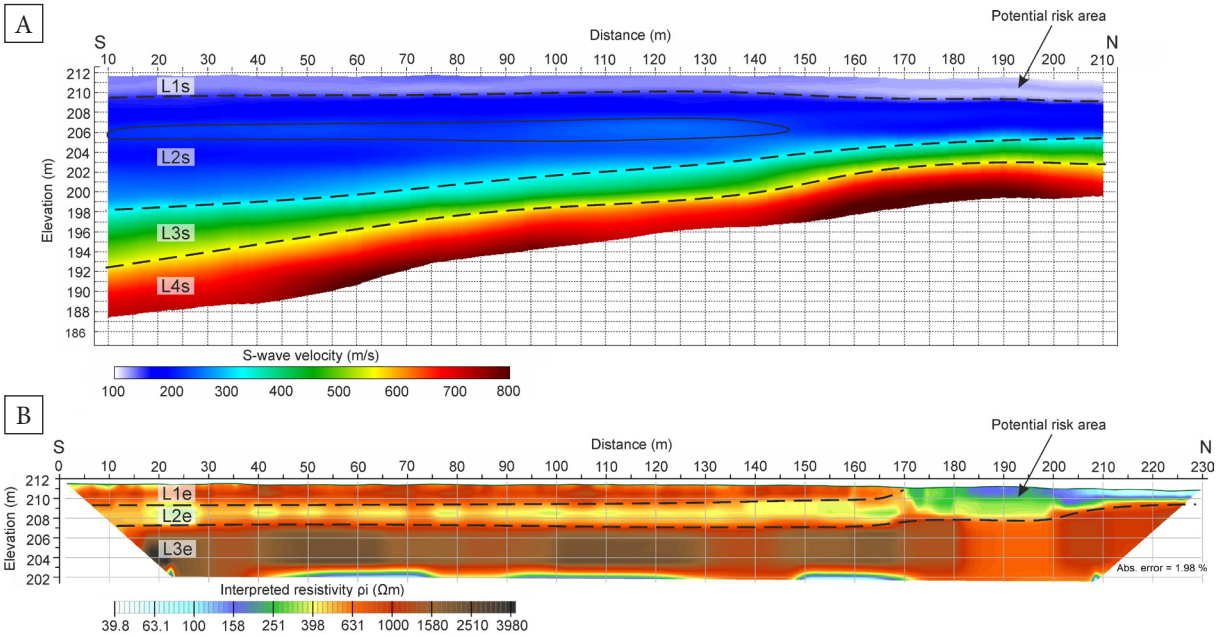

Fig. 6. *Results of the MASW-3 (A) and ERT-3 (B) geophysical measurements. Explanations: L1s – L4s – interpreted seismic layers, L1e – L3e – interpreted geoelectrical layers. The oval within L2s indicates a sublayer characterised by relatively higher S-wave velocities*

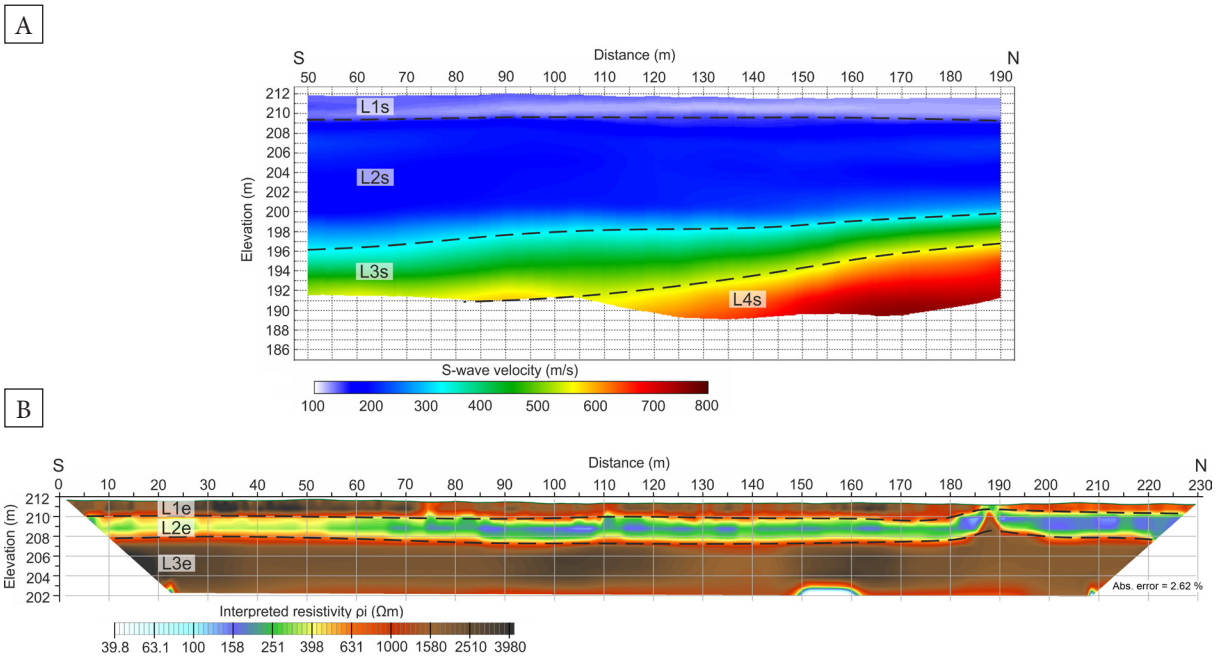

Fig. 7. *Results of the MASW-4 (A) and ERT-4 (B) geophysical measurements. Explanations: L1s – L4s – interpreted seismic layers, L1e – L3e – interpreted geoelectrical layers*

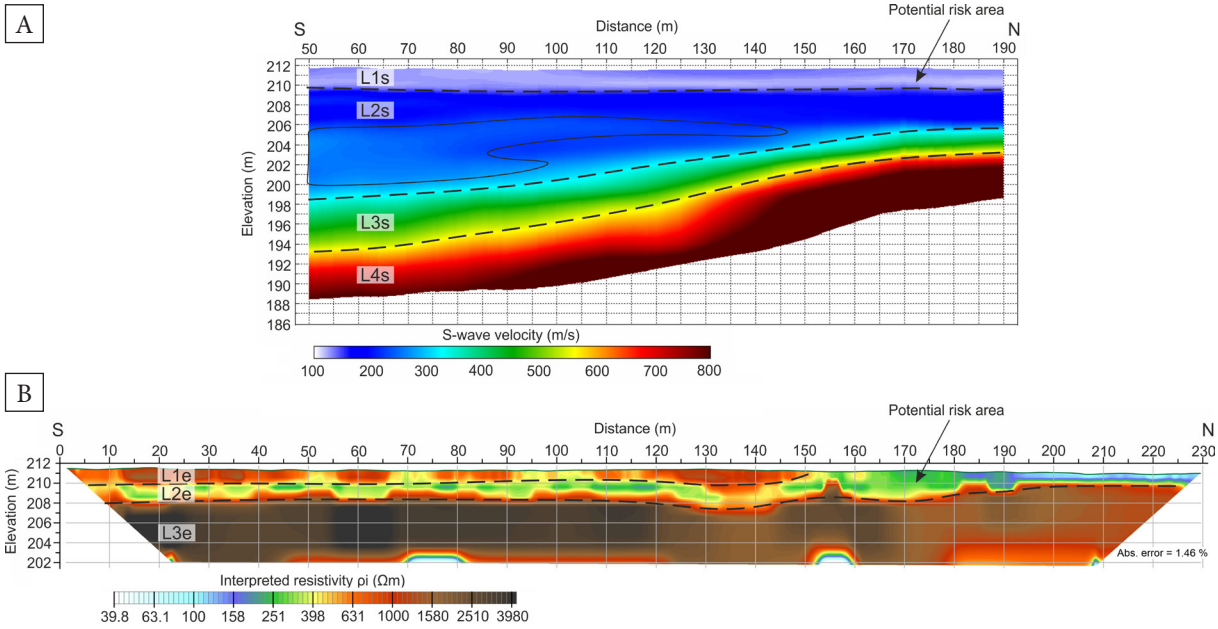

Fig. 8. *Results of the MASW-5 (A) and ERT-5 (B) geophysical measurements. Explanations: L1s – L4s – interpreted seismic layers, L1e – L3e – interpreted geoelectrical layers. The oval within L2s indicates a sublayer characterised by relatively higher S-wave velocities*

Generally, the geological medium can be divided into three nearly horizontal layers (L1e – L3e geoelectrical layers). The uppermost layer (L1e) is around 2 m thick and exhibits an average resistivity of approximately 1,000 Ω·m. On the ERT-4 section, the resistivity values within this layer reach up to 4,000 Ω·m. This layer does not occur throughout the study area. In its northern part, a zone of low resistivity values (up to 200 Ω·m) begins to appear. The second, underlying layer (L2e) exhibits low resistivity values, varying from 40 to 400 Ω·m, with an approximate thickness of 2 m. Towards the north, the layer increases in thickness to approximately 4 m (in ERT-1 section) and emerges at the surface in the northeast (sections ERT-1, ERT-2, ERT-3 and ERT-5). In the ERT-3 section, this layer has the highest resistivity values, which reach 400 Ω·m. The deepest, third layer (L3e) shows resistivity values in the range of several thousand ohm-metres, with low-resistivity zones occurring at the lower parts of all sections.

Integrated interpretation of MASW and ERT

The geophysical investigation integrating MASW and ERT conducted in the vicinity of Czernichów village provided valuable information about the vertical and lateral distribution of subsurface materials. The results of both methods were correlated with lithological data from borehole BH-1 (Figs. 2, 4), allowing the derived geophysical parameters to be linked to soil types. The study area consists mainly of soft, sandy soil layers overlying rigid limestone bedrock. Both methods show very good agreement with the borehole lithology and indicate that the subsurface is relatively homogeneous, with the distribution of physical parameters being similar across all profiles (Figs. 4–8). The first 2 m (interpreted layers L1s and L1e) are characterised by low shear wave velocities (below 120 m/s) and high resistivity values (more than 1,000 Ω·m). These parameters correspond to weak, very loose soils and dry sands.

Below this zone, a layer with lower resistivity is clearly evident in the ERT cross-sections (L2e). Its thickness is approximately 2 m. This layer, rich in clay, corresponds to the alluvial sediments identified in borehole BH-1. Along the ERT-3 profile, however, it shows the highest resistivity values, up to 400 Ω·m, indicating a lower clay content at this location. At the northern ends of all ERT sections,

low resistivity values extend to the surface, forming a near-surface anomaly with increased thickness. This anomaly is also visible in the MASW profiles as a decrease in velocity down to 100 m/s. It can be interpreted as very loose, weak, clay-dominated soil.

The third geoelectrical layer (L3e) is characterised by high resistivity values, reaching up to 4,000 Ω · m and can be correlated with the compact, poorly sorted sands and gravels found in borehole BH-1. Changes in resistivity in the layer highlight the increase of poorly sorted granular rock components and/or a different amount of pore water. Within the depth range of the geoelectrical second and third layers (from 2 to 8 m below ground level), S-wave velocities vary only slightly, with values of approximately 200 m/s (L2s). This suggests that the sands, alluvial soils, and sand–gravel mixtures present here, despite showing significant variations in resistivity, do not differ in terms of strength. Within this depth range, a thin sublayer characterised by relatively higher S-wave velocities (approximately 280 m/s) is observed, indicating the presence of stiffer material. This layer is not resolved in the westernmost profile (Fig. 7A), which may suggest lateral discontinuity or a reduction in thickness below the resolution limit of the MASW survey.

Below 8 m depth, a sharp increase in S-wave velocity is observed (L3s). Here, the velocities vary from 350 to 550 m/s. They correspond to very dense soil composed of sandy gravel (velocities up to 480 m/s) and silty clay (velocities above 480 m/s) as indicated in borehole BH-1. The layer with the highest S-wave velocity (greater than 600 m/s; L4s) can be associated with limestone, as confirmed by borehole BH-1. The interpreted depth of the limestone bedrock shows excellent agreement with the borehole data (Fig. 4), extending from the southwest (MASW-4 profile; Fig. 7), where the limestone occurs at its greatest depth of 22 m, to the northeast, where it rises to a shallow depth of 8 m (MASW-5 profile; Fig. 8). Together with the overlying layer, it forms a distinct NE-trending structure.

The ERT sections end at 10 m depth. At the bottom of each ERT cross-section, low-resistivity zones appear. These zones may reflect increased clay and/or water content at the base of the L3e layer and may also indicate the presence of an underlying silty clay layer below the investigation depth of the method, as suggested by the borehole BH-1 and by the transition to the deeper seismic layer L3s (Fig. 4). However, it may also be related to edge effects in the inverted resistivity model. Because this low-resistivity response coincides with the transition to very dense sandy gravel and silty clay recognised in the MASW interpretation, it is more likely to be related to geological structure than to inversion edge effects alone. Nevertheless, since the ERT sections terminate at this depth, some contribution from boundary effects in the inverted resistivity model cannot be excluded (Loke 2018). Interpretation in such a situation remains uncertain.

According to the National Earthquake Hazards Reduction Program (NEHRP) (Building Seismic Safety Council 2001a, 2001b) and International Building Code (IBC) (International Code Council 2009) soil classifications, the obtained S-wave velocities for limestone (600–800 m/s) are typical of stiff soil or soft rock rather than solid rock. Preliminary results from earlier P-wave seismic refraction measurements along profile 1 showed that the limestone has a P-wave velocity of 4,860 m/s (Borecka et al. 2014). Assuming a typical Poisson's ratio of 0.3 for the limestone, the S-wave velocity should be approximately 2,600 m/s. This discrepancy indicates that the MASW method underestimated the S-wave velocity of the limestone. While variations in fracturing, porosity, or saturation could change the estimated S-wave velocity, even a reasonable range of Poisson's ratio (0.20–0.35) still yields values much higher than those from MASW. In our case, an S-wave velocity of 800 m/s would imply a Poisson's ratio of 0.486, which is unrealistically high for a limestone. One possible explanation is the significant contrast in elastic properties between the soft soil and the rigid bedrock. This contrast led surface waves to propagate within a waveguide formed by the soil layers above the bedrock and the ground surface. As a result, the signal was received from the top of the bedrock rather than from the bedrock itself. Another potential explanation relates to the inverse problem: since the inversion of MASW

data is mathematically ill-posed, it may lead to non-unique solutions, which represents an inherent limitation of the method (Foti et al. 2009). In addition, strong velocity contrasts between layers reduces the sensitivity of the dispersion curves to deeper, high-velocity formations, increasing the uncertainty in the estimated S-wave velocity of the bedrock.

Analysis of the dispersion images from the study area indicates that the depth of the bedrock has a significant effect on the propagation of surface wave energy. This situation can be observed in Figure 2. When limestone occurs at greater depths, surface wave energy propagates to frequencies down to 7 Hz (Fig. 3A). In contrast, for shallow limestone, no clear energy is observed at frequencies below 11 Hz (Fig. 3B). However, this phenomenon still requires further investigation. Moreover, the presence of shallow stiff rock can generate higher modes of surface waves. Although these modes may provide additional constraints for inversion, they are difficult to interpret because they do not necessarily occur in sequential order. For example, what appears in Figure 3B as a higher mode could correspond to the first higher mode or to the second mode, and even interference between these and higher modes. In certain cases, surface wave energy may not propagate as the fundamental mode at all. Misidentifying the modes can result in an overestimation of S-wave velocities, because higher modes travel at faster phase velocities (Ivanov et al. 2011, Gao et al. 2015). One possible approach to reduce the ambiguity in dispersion images is to use multichannel analysis based on Love waves. Compared with Rayleigh waves, Love waves are generally less prone to generating higher modes of surface waves, which may result in a less ambiguous dispersion image. However, the acquisition of Love wave data requires both a horizontal seismic source and horizontal geophones. Such a configuration is generally more time-consuming and less practical in field conditions than the standard MASW setup employing a vertical impact source (e.g., a sledgehammer) and vertical geophones (Dal Moro 2014).

These factors illustrate that the interpretation of MASW data in areas with strong velocity contrasts and shallow bedrock should be treated with caution, and the obtained S-wave velocities should be considered as approximate estimates rather than exact values of the bedrock properties.

The relatively shallow investigation depth of ERT, compared with the seismic method, is attributable to the chosen Wenner array dimensions and the selected electrode spacing. This configuration was dictated by technical constraints – namely, the characteristics and limited power of the equipment used – and by the adopted roll-along acquisition procedure. In the present study, the roll-along technique required relocating the entire 95-electrode survey line at once and recording overlapping segments, whereas more recent measurement systems allow selective relocation of electrode subsets. For example, the SuperSting measurement system (manufactured by Advanced Geosciences, Inc.) permits roll-along by shifting 14 or 28 electrodes out of a 112-electrode layout (see e.g., Bania et al. 2024), although the exact capability depends on the hardware variant, the number of cables, and the number of electrodes that can be operated simultaneously. Such flexible roll-along implementations afford greater opportunities to extend the method's depth of investigation. Alternatively, larger sets of Wenner spacings or increased overall electrode spacing could have been employed by the authors; however, these options would have substantially increased the measurement time required for a single ERT profile and/or decreased the achievable depth resolution. The authors prioritised detailed characterisation of the near-surface strata while maintaining an optimal measurement duration and therefore adopted the described measurement geometry.

Groundwater was encountered in BH-1 at a depth of approximately 6.1 m, corresponding to an elevation of approximately 205.55 m (Fig. 2). This places the water table within the middle part of the L3e layer (Figs. 4–8), interpreted as sandy-gravel deposits. However, no distinct resistivity contrast within this layer can be directly linked to the groundwater table. This suggests that, under the studied hydrogeological conditions, the groundwater table does not form a well-defined geoelectrical boundary. A possible explanation is that the sandy fraction within the sand–gravel deposits promotes capillary rise and elevated pore

moisture above the groundwater table, leading to relatively uniform resistivity values throughout much of L3e. Consequently, the observed resistivity variability within this layer is interpreted primarily in terms of lithological heterogeneity within the sand–gravel sequence, although the influence of spatial variations in pore-water content cannot be entirely excluded.

Although the acquisition of five parallel 2D ERT profiles suggests the use of 3D inversion, this approach was not included in the interpretation. According to the practical guidelines provided by Loke (2003, 2018), pseudo-3D inversion based on parallel 2D lines is appropriate only when the spacing between neighbouring lines is relatively small, and in practice should not exceed approximately twice the unit electrode spacing. In the present survey, the inline electrode spacing was 1 m, whereas the spacing between adjacent profiles ranged from 15 to 25 m, which significantly exceeds the recommended limits for pseudo-3D inversion. Under such conditions, the resistivity distribution between the profiles is poorly constrained, and the inversion may generate artificial banding related to the acquisition geometry itself (Loke & Dahlin 2010). Test inversions were nevertheless performed; however, the resulting 3D models exhibited numerous artificial resistivity anomalies, particularly in the regions between adjacent profiles and near their boundaries. This effect was further amplified by lateral variability in the geological structure across the site. Therefore, the acquired dataset is not suitable for reliable 3D inversion.

CONCLUSIONS

An integrated geophysical survey using MASW and ERT was carried out to aid the geotechnical investigation in Czernichów. This study demonstrates the effectiveness of combining these techniques for site assessment. The results indicate that the combined application of MASW and ERT offers a cost-efficient approach to investigating subsurface conditions, reducing the need for expensive, invasive geotechnical tests, and can be applied for recognition in most geological settings.

The MASW method was able to image the subsurface to a maximum depth of approximately 24 m, allowing delineation of the depth and morphology of the limestone bedrock (Figs. 4–8). However, it was not successful in accurately resolving its velocity. In contrast, the ERT method resolved only the upper approximately 10 m and provided greater detail for the shallow layers. Both techniques clearly resolved the top 2 m. Between 2 and 10 m depth, MASW indicated a single, relatively homogeneous layer (L2s) with little variation in velocity (approximately 200 m/s). In comparison, ERT allowed clearer differentiation within the same depth, distinguishing alluvial soils (interpreted as the second layer, with resistivities of approximately 150 $\Omega \cdot m$) and sand–gravel mixtures (interpreted as the third layer, with resistivities greater than 1,000 $\Omega \cdot m$). The differences in lithological identification between the two methods arise from the different physical parameters they measure. ERT is sensitive to variations in clay content, porosity, and the presence of water, whereas MASW reflects variations in soil shear strength. In the study area, sands, alluvial soils, and sand–gravel mixtures have similar shear strengths but differ significantly in resistivity. Both methods indicate that the subsurface medium is characterised by a relatively uniform structure. However, a shallow anomalous zone extending to the surface is observed at the northern ends of profiles 1, 2, 3, and 5 (Figs. 4–6, 8). This zone is defined by a decrease in both S-wave velocity (down to approximately 100 m/s) and resistivity (down to approximately 30 $\Omega \cdot m$). In the ERT-1 cross-section, it correlates with alluvial soils (Fig. 4B). The observed changes in geophysical parameters suggest the presence of weaker alluvial soils with increased clay content, which may indicate a potential risk area requiring further geotechnical investigation. In the ERT-4 profile (Fig. 7B), this zone is not observed because the survey line does not extend far enough.

This research was partially funded by the subsidy granted to the AGH University of Krakow by the Ministry of Science and Higher Education and partially funded under the "Initiative of Excellence – Research University" program at AGH University of Krakow. We would like to express our appreciation to the anonymous reviewers for their valuable comments and feedback on the manuscript.

REFERENCES

Adenuga O.A. & Popoola O.I., 2020. Subsurface characterization using electrical resistivity and MASW techniques for suitable municipal solid waste disposal site. *SN Applied Sciences*, 2(9), 1549. https://doi.org/10.1007/s42452-020-03320-x.

Akinbiyi O.A., Oladunjoye M.A., Sanuade O.A. & Oyedeji O., 2019. Geophysical characterization and hydraulic properties of unconsolidated floodplain aquifer system in Wamako area, Sokoto State, north-western Nigeria. *Applied Water Science*, 9(8), 177. https://doi.org/10.1007/s13201-019-1065-y.

Akinsunmade A., Tomecka-Suchoń S. & Pysz P., 2020. Complex analysis of GPR signals for the delineation of subsurface subtle features. *Geology, Geophysics and Environment*, 45(4), 257–273. https://doi.org/10.7494/geol.2019.45.4.257.

Bania G. & Woźniak T., 2022. Subsurface imaging of fluvial deposits of the Wisła River valley in Kraków (southern Poland) by 2D ERT survey. *Geological Quarterly*, 66(3), 23. https://doi.org/10.7306/gq.1655.

Bania G., Mościcki W.J. & Golonka J., 2024. ERT field survey supported with numerical and analogue modeling applied to study a fragment of the Pieniny Klippen Belt (Spisz Pieniny Mountains, southern Poland). *Geological Quarterly*, 68(2), 22. https://doi.org/10.7306/gq.1750.

Borecka A., Kaczmarczyk R., Krokoszyński P., Ptaszek M., Stanisz J., Korzec K., Kret E., Tchórzewska S., Nowak P., Świątek M., Pękala M. & Dąbrowski J., 2014. *Dokumentacja geologiczno-inżynierska wraz z dokumentacją badań podłoża gruntowego sporządzona w celu określenia warunków geologiczno-inżynierskich dla projektowanej budowy eksperymentalnego wału przeciwpowodziowego na działce nr 796 w Czernichowie*. Akademia Górniczo-Hutnicza, Kraków [unpublished].

Boschetti F., Dentith M.C. & List R.D., 1996. Inversion of seismic refraction data using genetic algorithms. *Geophysics*, 61(6), 1715–1727. https://doi.org/10.1190/1.1444089.

Building Seismic Safety Council, 2001a. *NEHRP Recommended Provisions for Seismic Regulations for New Buildings and Other Structures, 2000 edition, Part 1: Provisions (FEMA 368)*. Federal Emergency Management Agency and the National Institute of Building Sciences, Washington.

Building Seismic Safety Council, 2001b. *NEHRP Recommended Provisions for Seismic Regulations for New Buildings and Other Structures, 2000 edition, Part 2: Commentary (FEMA 369)*. Federal Emergency Management Agency and the National Institute of Building Sciences, Washington.

Burger H.T., Sheehan A.F. & Jones C.H., 2006. *Introduction to Applied Geophysics: Exploring the Shallow Subsurface*. Cambridge University Press, Cambridge.

Cichostępski K. & Dec J., 2021. Estimation of shallow sulphur deposit resources based on reflection seismic studies and well logging. *Energies*, 14(17), 5323. https://doi.org/10.3390/en14175323.

Cichostępski K., Dec J. & Kwietniak A., 2019a. Relative amplitude preservation in high-resolution shallow reflection seismic: Acase study from Fore-Sudetic Monocline, Poland. *Acta Geophysica*, 67(1), 77–94. https://doi.org/10.1007/s11600-018-00242-6.

Cichostępski K., Dec J. & Kwietniak A., 2019b. Simultaneous inversion of shallow seismic data for imaging of sulfurized carbonates. *Minerals*, 9(4), 203. https://doi.org/10.3390/min9040203.

Cichostępski K., Dec J., Golonka J. & Waśkowska A., 2024. Shallow seismic refraction tomography images from the Pieniny Klippen Belt (southern Poland). *Minerals*, 14(2), 155. https://doi.org/10.3390/min14020155.

Clayton C.R.I., Matthews M.C. & Simons N.E., 1995. *Site Investigation* (2nd ed.). Wiley-Blackwell, Hoboken.

Cosenza P., Marmet E., Rejiba F., Cui Y.J., Tabbagh A. & Charlery Y., 2006. Correlations between geotechnical and electrical data: Acase study at Garchy in France. *Journal of Applied Geophysics*, 60 (3–4), 165–178. https://doi.org/10.1016/j.jappgeo.2006.02.003.

Craig M. & Hayashi K., 2016. Surface wave surveying for near-surface site characterization in the East San Francisco Bay Area, California. *Interpretation*, 4(2), SQ59–SQ69. https://doi.org/10.1190/INT-2015-0227.1.

Craig M., Hayashi K. & Kozci Ö., 2021. Active and passive seismic surface wave methods for levee assessment in the Sacramento–San Joaquin Delta, California, USA. *Near Surface Geophysics*, 19(2), 141–154. https://doi.org/10.1002/nsg.12144.

Dahlin T., 1996. 2D Resistivity surveying for environmental and engineering applications. *First Break*, 14(7), 275–284. https://doi.org/10.3997/1365-2397.1996014.

Dal Moro G., 2014. *Surface Wave Analysis for Near Surface Applications*. Elsevier, Amsterdam.

Dal Moro G., Pipan M. & Gabrielli P., 2007. Rayleigh wave dispersion curve inversion via genetic algorithms and marginal posterior probability density estimation. *Journal of Applied Geophysics*, 61(1), 39–55. https://doi.org/10.1016/j.jappgeo.2006.04.002.

Elwaseif M. & Slater L., 2010. Quantifying tomb geometries in resistivity images using watershed algorithms. *Journal of Archaeological Science*, 37(7), 1424–1436. https://doi.org/10.1016/j.jas.2010.01.002.

Foti S., Comina C., Boiero D. & Socco L.V., 2009. Non-uniqueness in surface-wave inversion and consequences on seismic site response analyses. *Soil Dynamics and Earthquake Engineering*, 29(6), 982–993. https://doi.org/10.1016/j.soildyn.2008.11.004.

Foti S., Parolai S., Albarello D. & Picozzi M., 2011. Application of surface-wave methods for seismic site characterization. *Surveys in Geophysics*, 32(6), 777–825. https://doi.org/10.1007/s10712-011-9134-2.

Gao L., Xia J., Pan Y. & Xu Y., 2015. Reason and condition for mode kissing in MASW method. *Pure and Applied Geophysics*, 173(5), 1627–1638. https://doi.org/10.1007/s00024-015-1208-5.

Gołębiowski T., Pasierb B., Porzucek S. & Łój M., 2018. Complex prospection of medieval underground salt chambers in the village of Wiślica, Poland. *Archaeological Prospection*, 25(3), 243–254. https://doi.org/10.1002/arp.1706.

Golonka J., 1981. *Objaśnienia do mapy geologicznej Polski w skali 1:200 000: Arkusz Bielsko-Biała*. Wydawnictwa Geologiczne, Warszawa.

Golonka J., Waśkowska A., Cichostępski K., Dec J., Pietsch K., Łój M., Bania G., Mościcki W.J. & Porzucek S., 2022. Mélange, flysch and cliffs in the Pieniny Klippen Belt (Poland): An overview. *Minerals*, 12(9), 2022, 1149. https://doi.org/10.3390/min12091149.

Harba P., Pilecki Z. & Krawiec K., 2019. Comparison of MASW and seismic interferometry with use of ambient noise for estimation of S-wave velocity field in landslide subsurface. *Acta Geophysica*, 67(6), 1875–1883. https://doi.org/10.1007/s11600-019-00344-9.

Hayashi K., 2012. Analysis of surface-wave data including higher modes using the genetic algorithm. [in:] Hryciw R.D., Athanasopoulos-Zekkos A. & Yesiller N. (eds.), *GeoCongress 2012: State of the Art and Practice in Geotechnical Engineering, March 25–29, 2012, Oakland, California, USA*, Geotechnical Special Publication, 225, American Society of Civil Engineers, 2776–2785. https://doi.org/10.1061/9780784412121.284.

Hubbard J.L., 2009. *Use of Electrical Resistivity and Multichannel Analysis of Surface Wave Geophysical Tomography in Geotechnical Site Characterization of Dam*. The University of Texas at Arlington [MSc thesis].

Ikhane P.R., Omosanya K.O., Akinmosin A.A., Odugbesan A.B., 2012. Electrical resistivity imaging (ERI) of slope deposits and structures in some parts of eastern Dahomey Basin. *Journal of Applied Sciences*, 12(8), 716–726. https://doi.org/10.3923/jas.2012.716.726.

International Code Council, 2009. *ICC IBC (2009): International Building Code*. ICC, Country Club Hills, Illinois. https://archive.org/details/gov.law.icc.ibc.2009.

Ivanov J., Miller R.D., Lacombe P., Johnson C.D. & Lane J.W., 2006. Delineating a shallow fault zone and dipping bedrock strata using multichannel analysis of surface waves with a land streamer. *Geophysics*, 71(5), A39–A42. https://doi.org/10.1190/1.2227521.

Ivanov J., Miller R.D. & Tsoflias G., 2008. Some practical aspects of MASW analysis and processing. [in:] *21st Symposium on the Application of Geophysics to Engineering and Environmental Problems 2008: April 6–10, 2008, Philadelphia, Pennsylvania, USA*, Environmental and Engineering Geophysical Society, 1186–1198. https://doi.org/10.4133/1.2963228.

Ivanov J., Miller R.D., Peterie S., Zeng C. Xia J. & Schwenk T., 2011. Multi-channel analysis of surface waves (MASW) of models with high S-wave velocity contrast. [in:] *Society of Exploration Geophysicists International Exposition and 81st Annual Meeting 2011 (SEG San Antonio 2011): 18–23 September 2011, San Antonio, Texas, USA*, *SEG Technical Program Expanded Abstracts 2011*, Society of Exploration Geophysicists (SEG), Houston, 1384–1390. https://doi.org/10.1190/1.3627461.

Loke M.H., 2003. *Rapid 2D Resistivity & IP Inversion Using the Least-Squares Method*. Geotomo Software, Penang, Malaysia.

Loke M.H., 2018. *Tutorial: 2-D and 3-D Electrical Imaging Surveys*. Geotomo Software, Penang, Malaysia.

Loke M.H. & Dahlin T., 2010. Methods to reduce banding effects in 3-D resistivity inversion. [in:] *Near Surface Geoscience 2010: 16th European Meeting of Environmental and Engineering Geophysics: 6–8 September 2010, Zurich, Switzerland*, European Association of Geoscientists and Engineers (EAGE), Houten, The Netherlands, 76–80. https://doi.org/10.3997/2214-4609.20144781.

Loke M.H., Ackworth I. & Dahlin T., 2003. A comparison of smooth and blocky inversion methods in 2D electrical imaging surveys. *Exploration Geophysics*, 34(3), 182–187. https://doi.org/10.1071/EG03182.

Łój M., Porzucek S., Bania G. & Cichostępski K., 2025. Integrated geophysical research in a profile crossing the mélange belt within the Pieniny Klippen Belt – a case study. *Annales Societatis Geologorum Poloniae*, 95(1), 17–28. https://doi.org/10.14241/asgp.2025.02.

Matys Grygar T., Elznicová J., Tůmová Š., Faměra M., Balogh M. & Kiss T., 2016. Floodplain architecture of an actively meandering river (the Ploučnice River, the Czech Republic) as revealed by the distribution of pollution and electrical resistivity tomography. *Geomorphology*, 254, 41–56. https://doi.org/10.1016/j.geomorph.2015.11.012.

Mayne P.W. & Rix G.J., 1993. Correlation between S-wave velocity and cone tip resistance in natural clays. *Soils and Foundation*, 35(2), 107–110. https://doi.org/10.3208/sandf1972.35.2_107.

Mościcki W.J., Bania G., Ćwiklik M. & Borecka A., 2014. DC resistivity studies of shallow geology in the vicinity of Vistula River flood bank in Czernichow village (near Krakow in Poland). *Studia Geotechnica et Mechanica*, 36(1), 63–70. https://doi.org/10.2478/sgem-2014-0008.

Naveen B.P., Sithatam T.G., Sivapullaiah P.V. & Kumar S., 2021. Geophysical techniques for characterisation of municipal solid waste landfills. *Waste and Resource Manangement*, 174(3), 78–96. https://doi.org/10.1680/jwarm.20.00022.

Olona J., Pulgar J.A., Fernández-Viejo G., López-Fernández C. & González-Cortina J.M., 2010. Weathering variations in a graniticmassif and related geotechnical properties through seismic and electrical resistivity methods. *Near Surface Geophysics*, 8(6), 585–599. https://doi.org/10.3997/1873-0604.2010043.

Park C., 2013. MASW for geotechnical site investigation. *The Leading Edge*, 32(6), 656–662. https://doi.org/10.1190/tle32060656.1.

Park C.B. & Taylor C., 2010. 3D MASW characterization of sinkhole: A pilot study at USF Geology Park, Tampa, FL. [in:] *23rd Symposium on the Application of Geophysics to Engineering and Environmental Problems 2010 (SAGEEP 2010): 11–15 April 2010, Keystone, Colorado, USA*, Environmental and Engineering Geophysical Society (EEGS), Denver, CO, 498–507.

Park C.B., Miller R.D. & Xia J., 1999. Multichannel analysis of surface waves. *Geophysics*, 64(3), 800–808. https://doi.org/10.1190/1.1444590.

Ryłko W. & Paul Z., 2013. *Szczegółowa mapa geologiczna Polski w skali 1:50 000: Arkusz Kalwaria Zebrzydowska (995)*. Państwowy Instytut Geologiczny – Państwowy Instytut Badawczy, Warszawa.

Samui P. & Sitharam T., 2010. Correlation between SPT, CPT and MASW. *International Journal of Geotechnical Engineering*, 4(2), 279–288. https://doi.org/10.3328/IJGE.2010.04.02.279-288.

Smith R.C. & Sjogren D.B., 2006. An evaluation of electrical resistivity imaging (ERI) in Quaternary sediments, southern Alberta, Canada. *Geosphere*, 2(6), 287–298. https://doi.org/10.1130/GES00048.1.

Taipodia J., Dey A. & Baglari D., 2018. Influence of data acquisition and signal preprocessing parameters on the resolution of dispersion image from active MASW survey. *Journal of Geophysics and Engineering*, 15(4), 1310–1326. https://doi.org/10.1088/1742-2140/aaaf4c.

Telford W.M., Geldart L.P. & Sheriff R.E., 1990. *Applied Geophysics* (2nd ed.). Cambridge University Press, London.

Woźniak T. & Bania G., 2019a. Analysis of the tectonic and sedimentary features of the southern margin of the Krzeszowice Graben in Southern Poland based on an integrated geoelectrical and geological studies. *Journal of Applied Geophysics*, 165, 60–76. https://doi.org/10.1016/j.jappgeo.2019.04.010.

Woźniak T. & Bania G., 2019b. Integrated geoelectrical and geological data sets for shallow structure characterization of the southern margin of the Krzeszowice Graben (Southern Poland). *Data in Brief*, 25, 104157. https://doi.org/10.1016/j.dib.2019.104157.

Woźniak T., Bania G., Mościcki W.J. & Ćwiklik M., 2018. Electrical resistivity tomography (ERT) and sedimentological analysis applied to investigation of Upper Jurassic limestones from the Krzeszowice Graben (Kraków Upland, southern Poland). *Geological Quarterly*, 62(2), 287–302. https://doi.org/10.7306/gq.1403.

Xia J., Miller R.D. & Park C.B., 1999. Estimation of near-surface S-wave velocity by inversion of Rayleigh waves. *Geophysics*, 64(3), 691–700. https://doi.org/10.1190/1.1444578.

Xia J., Miller R.D., Park C.B. & Ivanov J., 2000. Construction of 2-D vertical S-wave velocity field by the multichannel analysis of surface wave technique, [in:] Powers M.H., Ibrahim A.-B. & Cramer L. (eds.), *Proceedings of the Symposium on the Application of Geophysics to Engineering and Environmental Problems: February 20–24, 2000, Arlington, VA*, Environmental and Engineering Geophysical Society, Wheat Ridge, CO, 1197–1206. https://doi.org/10.4133/1.2922726.

Yamanaka H. & Ishida H., 1996. Application of Generic algorithms to an inversion of surface-wave dispersion data. *Bulletin of Seismological Society of America*, 86(2), 436–444. https://doi.org/10.1785/BSSA0860020436.

Zhao R., Anderson N. & Sun J., 2020. Geophysical investigation of a solid waste disposal site using integrated electrical resistivity tomography and multichannel analyses of surface waves methods. *Journal of Geoscience and Environment Protection*, 8(3), 55–69. https://doi.org/10.4236/gep.2020.83005.